Development of a High-Throughput Microwave Imaging System for Concealed Weapons Detection

William F. Moulder, James D. Krieger, Janusz J. Majewski, Charles M. Coldwell, Huy T. Nguyen,
Denise T. Maurais-Galejs, Thomas L. Anderson, Pierre Dufilie and Jeffrey S. Herd

MIT Lincoln Laboratory

william.moulder@ll.mit.edu

Abstract—A video-rate microwave imaging aperture for concealed threat detection can serve as a useful tool in securing crowded, high foot traffic environments. Realization of such a system presents two major technical challenges: 1) implementation of an electrically large antenna array for capture of a moving subject, and 2) fast image reconstruction on cost-effective computing hardware. This paper presents a hardware-efficient multistatic array design to address the former challenge, and a compatible fast imaging technique to address the latter. Prototype hardware which forms a partition of an imaging aperture is also discussed. Using this hardware, it is shown that the proposed array design can be used to form high-fidelity 3D images, and that the presented image reconstruction technique can form an image of a human-sized domain in $\leq 0.1s$ with low cost computing hardware.

Index Terms—Microwave imaging, multistatic radar, Fast Fourier Transform (FFT).

I. INTRODUCTION

Near-field microwave imaging is a non-ionizing and cost-effective sensing modality for variety of applications, including Non-Destructive Evaluation (NDE) [1], medical diagnostics [2], and detection of concealed weapons [3]–[5]. In the latter application, a need exists for a practical system that can image subjects in high foot traffic environments, such as mass transit systems, stadiums, and large public events. As notionally illustrated in Fig. 1, a microwave imaging aperture could be arranged in corridors, or placed on walls to screen subjects for concealed threats. In order to handle a potentially constant stream of subjects in motion, the system must measure a subject very quickly (on the order of 10's of milliseconds), and reconstruct microwave images of a subject at video rate ($\geq 10Hz$).

These system requirements present two major challenges. The first challenge is cost-effective realization of an electrically large antenna array. The fast acquisition requirement implies that the system must be fully electronic (e.g., it samples the scene with no moving sensors). Furthermore, for proper near-field illumination of a human subject, the array must be roughly the size of the subject (1-2m). For a high resolution system operating in the 10's of GHz, this implies an aperture size in excess of 100λ. A well-known paradigm that mitigates this challenge is multistatic sampling [4], [6]–[11]. Such array topologies use transmitters and receivers that are not co-located, maximizing diversity of spatial sampling.
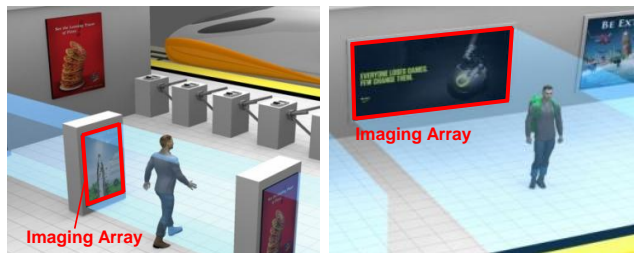

Fig. 1. Potential implementations of video rate microwave imaging system for concealed threat detection.

The second challenge that the proposed system presents is video rate image formation. The well-known backprojection algorithm [4] can be used with any multistatic configuration, but its computational demands are extreme. Fast Fourier Transform (FFT) imaging has long been used to efficiently construct images sampled with monostatic sampling schemes [3], however, this formulation cannot be used directly with multistatic sampled data. Recently, a modified FFT imaging formulation for multistatic arrays was presented [8]. While this formulation represents a tremendous improvement over backprojection, it still requires use of multiple sub-domains and interpolations to image a human subject, adding substantial overhead to the FFT imaging formulation.

In response to these challenges, Section II of this paper presents a multistatic array design for hardware efficient realization of an electrically large aperture, while Section III presents a fast image reconstruction technique for the multistatic array. As described in Section III, design of the array and imaging algorithm are inter-related. Section IV presents prototype hardware that represents a portion of an imaging aperture (including switched antennas, transceiver, data recorder) and a processor for fast image reconstruction. In that section, it is shown that the array topology can be used for high-fidelity 3D microwave imaging. Further, it is shown that the fast imaging technique can reconstruct a human-sized image domain in $\leq 0.1s$ on relatively inexpensive computing hardware.

II. ARRAY DESIGN

A. Background: Monostatic Imaging

While the presented array design employs multistatic sampling, its explanation is aided by discussion of monostatic
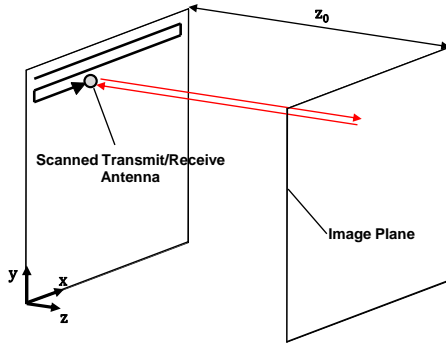
Fig. 2. Notional description of a monostatic imaging scheme.

Fig. 3. Example (1m size) of multistatic array layout.

imaging. As seen in Fig. 2, a monostatic imaging setup employs a co-located transmit/receive antenna that is scanned (either mechanically or electronically) in a plane. Typically, the scene is sampled with a regular grid of phase centers (antenna locations). A grid spacing of $> \lambda/4$ samples the scene without spatial aliasing, however, given the limited beamwidth of typical antenna elements, a spacing of $\lambda/2$ is usually sufficient. One advantage of monostatic sampling is that it is readily compatible with FFT imaging, an extremely computationally efficient approach to microwave image reconstruction. Using this approach, a 2D image can be formed with the following expression [3]:

$$I(x,y) = IFFT_{2D}[FFT_{2D}[s(n_x, n_y)]e^{-j\sqrt{4k^2 - k_x^2 - k_y^2}z_0}]$$

(1)

where $s(n_x, n_y)$ is the matrix of measured reflections and z_0 is the spacing between the aperture and measurement planes. As the data is taken on a 2D spatial grid, n_x and n_y are column and row indices of the grid. Spatial coordinates (x,y) lie on the image plane, and correspond to the position of a sampled phase center with indices (n_x, n_y). Equation (1) can, of course, be evaluated at multiple frequencies, and coherently summed within an image plane. For 3D imaging, multiple image planes can be evaluated to construct a volumetric domain in slices. Alternatively, a formulation similar to (1) using 3D FFTs can be used [3], but this requires interpolations which may be computationally expensive.

While an electronically switched monostatic imager for capture of a moving subject could conceivably be realized, it would require an extreme number of antenna elements. For example, a system operating at 30 GHz would require about 40,000 elements per $1m^2$. Hence, use of a multistatic array topology, such as the one presented in the next subsection, is critical.

B. Multistatic Array Topology

Multistatic array topologies can be used to dramatically reduce the number of antenna elements required in a large imaging aperture, mitigating hardware costs [4], [5], [7]. A multistatic array with N_{Tx} transmit antennas and N_{Rx} receive antennas can form up to $N_{Tx}N_{Rx}$ spatially diverse phase
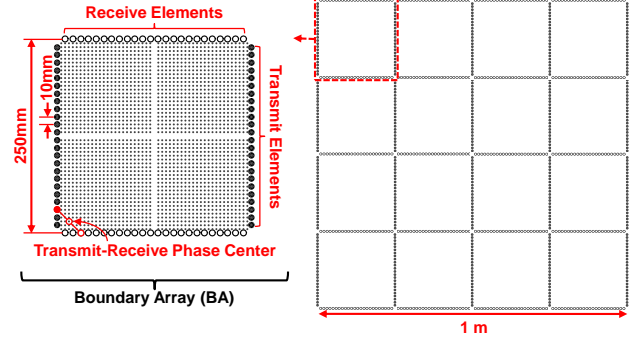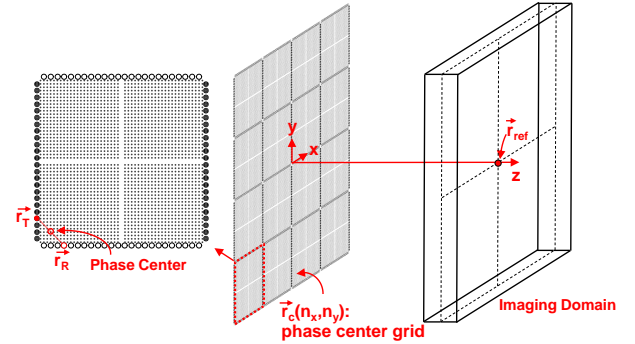

Fig. 4. Notional depiction of 1m multistatic array imaging a scene.

centers since the transmit and receive antennas are not co-located.

The presented multistatic array topology is depicted in Fig. 3. The elementary unit of the design is the Boundary Array (BA) [7], a topology that employs four linear arrays that cover its perimeter. In the depicted example, the arrays on the BA's left and right side are transmitters, while the arrays on its top and bottom are receivers. The interior of the BA is empty. Assuming that the BA is sized such that its side length is short compared to imaging range, each transmit-receive element pair forms an effective phase center, which lies at the midpoint of the two elements. If every transmit-receive pair is sampled (e.g., via rapidly switching between the elements), a grid of phase centers is formed. With exception of the missing phase centers in the grid's middle row and column, the grid is a uniformly spaced block. In the depicted example, the elements are spaced by $10mm$, or 1λ at 30 GHz. The resultant phase center grid, then, is spaced by 0.5λ. It is noted that depicted BA cell contains 48 transmit antennas and 48 receive antennas, to form 48^2 or 2304 phase centers. As seen in Fig. 3, the full array topology is a tiled arrangement of BAs. Each BA samples the set of phase centers within its extent, resulting in a regular grid of phase centers (with no redundancy), that covers the 1m aperture. The grid excludes points along one row and column in the center of each BA tile, and at the positions of the antenna elements. However, these "missing phase centers" are small in number, compared to the populated phase center set,

and thus do not have a major effect on image quality. The $1m$ aperture example contains 480 transmit antennas, 480 receive antennas, and forms 36,864 phase centers.

The presented topology shares some similarities with the one presented in [4]. However, the sampling scheme is a critical difference between the two designs. In the design depicted in Fig. 3, transmit-receive sampling occurs only within a given BA unit cell. In other words, a linear transmit array never communicates with a non-adjacent receive array. This restricts the distance between transmit-receive pairs, which, as will be discussed in the next section, is critical to the fast imaging technique. In contrast, the design employed in [4] samples with no such restriction, which would be problematic for the presented imaging technique.

III. FAST IMAGING TECHNIQUE

A. Formulation

While Equation (1) provides efficient image reconstruction for *monostatic* sampled datasets, fast image formation remains a challenge for multistatic data. In this section, a fast imaging technique that is compatible with the multistatic array depicted in Fig. 3 is presented. For each frequency point, captured scene reflection data is formatted into a matrix $s(n_x, n_y)$, where n_x and n_y are phase center indices (see Fig. 4) corresponding to locations along the $x-$ and $y-$axes. Entries in this matrix corresponding to the "missing phase centers" mentioned in Section II-B are set to zero. We define a reference point at the center of the imaging domain, whose position is given by $\overrightarrow{r}_{ref}$, as depicted in Fig. 4. The data then undergoes an multistatic-to-monostatic correction, which makes the multistatic data approximate a reflection set taken by a hypothetical monostatic aperture. For a dataset $s(n_x, n_y)$, the corrected dataset $\hat{s}(n_x, n_y)$ is given by:

$$\hat{s}(n_x, n_y) = s(n_x, n_y) \frac{R_o(n_x, n_y)}{R_u(n_x, n_y)}. \quad (2)$$

$R_u(n_x, n_y)$ is the calculated reflection set that the design depicted in Fig. 3 would receive if it probed a scene that contained only a point scatterer placed at $\overrightarrow{r}_{ref}$:

$$R_u(n_x, n_y) = e^{-jk|\overrightarrow{r}_T(n_x, n_y) - \overrightarrow{r}_{ref}|} e^{-jk|\overrightarrow{r}_{ref} - \overrightarrow{r}_R(n_x, n_y)|}. \quad (3)$$

$R_o(n_x, n_y)$ is the calculated reflection set that would be received by a hypothetical *monostatic* aperture imaging the single point scatterer scene, where sampling takes place on the multistatic aperture's phase center grid ($\overrightarrow{r}_c$, see Fig. 4):

$$R_o(n_x, n_y) = e^{-j2k|\overrightarrow{r}_c(n_x, n_y) - \overrightarrow{r}_{ref}|}. \quad (4)$$

The corrected data $\hat{s}(n_x, n_y)$ is then zero padded to size 2^N for FFT processing. Following this, the image is efficiently formed by applying Equation (1) to the corrected data. Substituting (2) into (1) gives a complete form of the multistatic imaging technique:
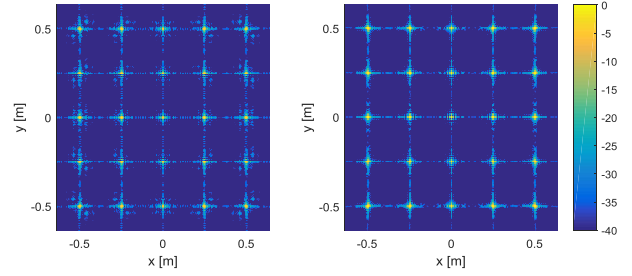

Fig. 5. Simulated image of 25 point scatterers imaged at range 1.5m, with array layout depicted in Fig. 3. Left: image formed with Equation (5) (Fourier Imaging); Right: image formed with Equation (7) (Backprojection).
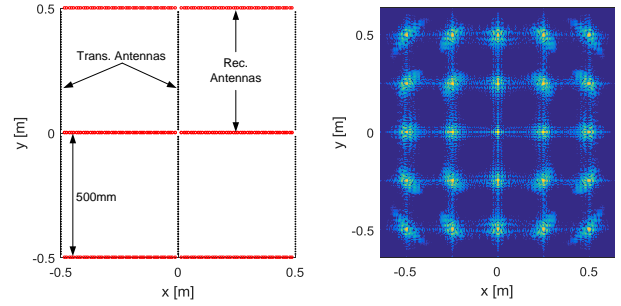

Fig. 6. Left: layout of 1m multistatic aperture with 0.5m BA tiles. Right: simulated image of 25 point scatterers at range 1.5m, using Equation (5) for reconstruction. Dynamic range of image is 40dB.

$$I(x, y) = IFFT_{2D}[FFT_{2D}[s(n_x, n_y) \frac{R_o(n_x, n_y)}{R_u(n_x, n_y)}].$$
$$e^{-j\sqrt{4k^2 - k_x^2 - k_y^2} z_0}]. \quad (5)$$

B. Comparison with Backprojection Imaging

Fig. 5 provides a set of simulated images of 25 point scatterers imaged at range 1.5m, with array layout depicted in Fig. 3. In the analysis, a frequency span of 24-30 GHz (32 steps) was assumed. Simulated data was obtained via a simple scattering model, where the reflection between a transmit and
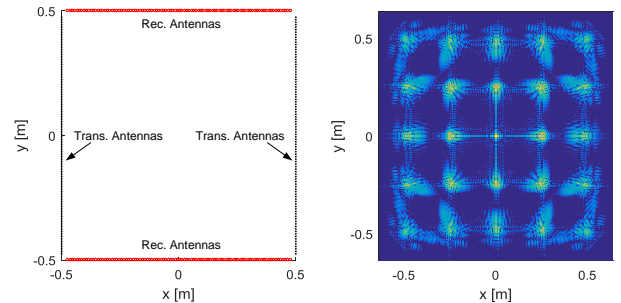

Fig. 7. Left: layout of 1m multistatic aperture made up of single BA. Right: simulated image of 25 point scatterers at range 1.5m, using Equation (5) for reconstruction. Dynamic range of image is 40dB.

receive antenna pair due to a set of point scatterers is given by:

$$s(n_{Tx}, n_{Rx}) = \sum_{n_s=1}^{N_s} e^{-jk|\overrightarrow{r}_s - \overrightarrow{r}_{Tx}|} e^{-jk|\overrightarrow{r}_s - \overrightarrow{r}_{Rx}|}, \quad (6)$$

where N_s is the number of point scatterers, $\overrightarrow{r}_s$ is the position of a scatterer, $\overrightarrow{r}_{Tx}$ is transmitter position, and $\overrightarrow{r}_{Rx}$ is receiver position.

In the left image of Fig. 5, the data processed with the multistatic FFT imaging technique (Equation (5)). In the right image, the commonly used backprojection technique was used, where $I(\overrightarrow{r_v})$, the image at position $\overrightarrow{r_v}$ is given by:

$$I(\overrightarrow{r_v}) = \sum_{n_{Tx}=1}^{N_{Tx}} \sum_{n_{Rx}=1}^{N_{Rx}} s(n_{Tx}, n_{Rx}) e^{jk|\overrightarrow{r}_v - \overrightarrow{r}_{Tx}|} \\ e^{jk|\overrightarrow{r}_{Rx} - \overrightarrow{r}_v|}. \quad (7)$$

It is noted that $s(n_{Tx}, n_{Rx})$ is the matrix of measured reflections and (n_{Tx}, n_{Rx}) is a set of transmit/receive antenna indices. As seen, the simulated images are quite similar, with only minor differences appearing near the floor of the images' dynamic range (40dB). However, the image formed with the multistatic FFT imaging technique can be reconstructed with far fewer computational resources (or much less processing time, for a given computer). To quantify the differences in processing load in a manner that is independent of computing hardware, the complexity of each technique was evaluated using computational workload values provided in [12]. According to this analysis, formation of the image depicted in Fig. 5 requires 0.57 GFLOP (Giga-Floating Point Operations) using the fast imaging technique presented in the preceding section, while a vectorized implementation of backprojection requires 512 GFLO, a difference of nearly 3 orders of magnitude. It is noted that in both images, the image plane was formed with 256x256 pixels.

C. Co-design of Array and Imaging Algorithm

The image reconstruction technique described in the preceding subsection places constraints on the the multistatic array topology that can be used. First, the topology must produce data that can be formatted in a regular grid of phase centers, for compatibility with the FFT. Second, the spacing between transmit-receive antenna pairs must be restricted for the approximation described by Equation (2) to be valid. Simulations are presented in this section to illustrate this point.

One might consider a modified version of the array depicted in Fig. 3 that uses a set of four 500mm BA tiles to form a 1m aperture, rather than a set of sixteen 250mm tiles. Fig. 6 depicts a layout where larger 500mm tiles are used. Additionally, Fig. 6 depicts a simulated image of 25 point scatterers (same scene as image in Fig. 5) where the multistatic FFT imaging technique was used. As seen, compared to the case where 250mm tiles were used, the version with 500mm tiles produces distorted images of the point scatterers. This
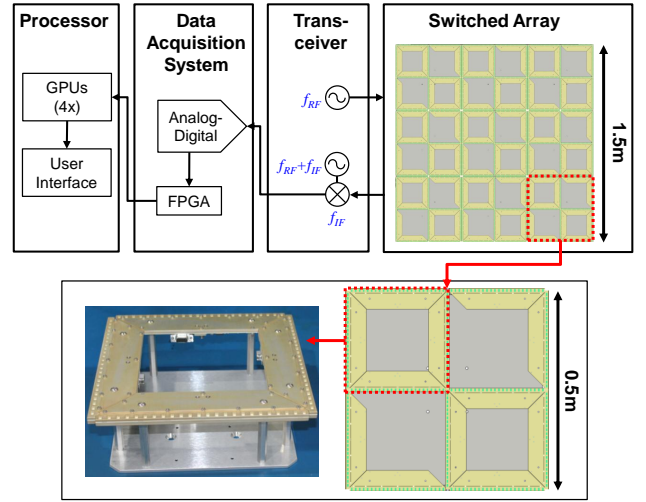

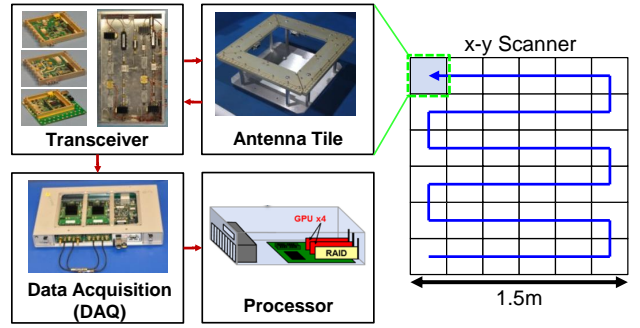Fig. 8. Block diagram of envisioned 1.5m aperture system.

Fig. 9. Prototype single tile system.

is due to the fact the the larger transmit-receive antenna separation degrades the approximation of Equation (2). This effect is even more pronounced when the case of Fig. 7 is considered, where a single 1m BA is used for imaging.

IV. PROTOTYPE SYSTEM AND MEASUREMENTS

Fig. 8 provides a block diagram of an envisioned imaging system that uses the design concepts discussed in Sections II and III. The system has four major subsystems: 1) a 1.5m switched array, whose layout is based on the topology described in Section II; 2) a transceiver, which provides frequency swept stimulus from 24-30 GHz, and downconverts reflected signals to an Intermediate Frequency (IF); 3) a Data Acquisition System (DAQ), which digitizes the IF; 4) a processor, which is a Commercial Off-The-Shelf (COTS) computer equipped with Graphics Processing Units (GPUs).

As an intermediate step toward realization of the system depicted in Fig. 8, a single tile version of the system was constructed and measured. Fig. 9 provides a block diagram of the prototype single tile system. The system includes a single BA antenna, a transceiver, a DAQ unit, and a processor. Operation of the fabricated BA antenna tile is described in [13]. The transceiver provides a stepped frequency stimulus
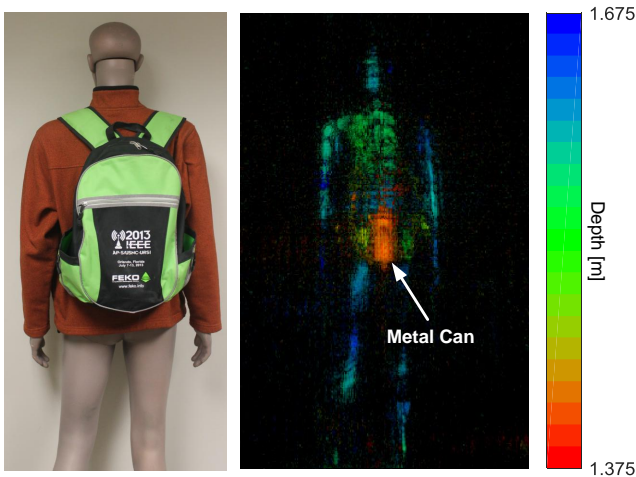
Fig. 10. Photo and microwave image of metalized mannequin concealing metal can in backpack (rear view).
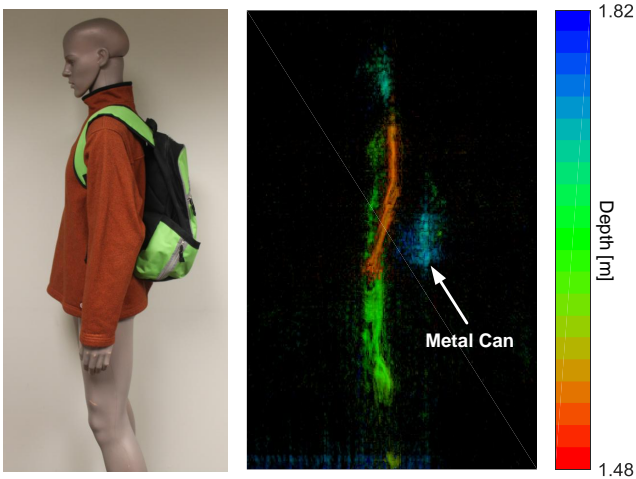

Fig. 11. Photo and microwave image of metalized mannequin concealing metal can in backpack (side view).
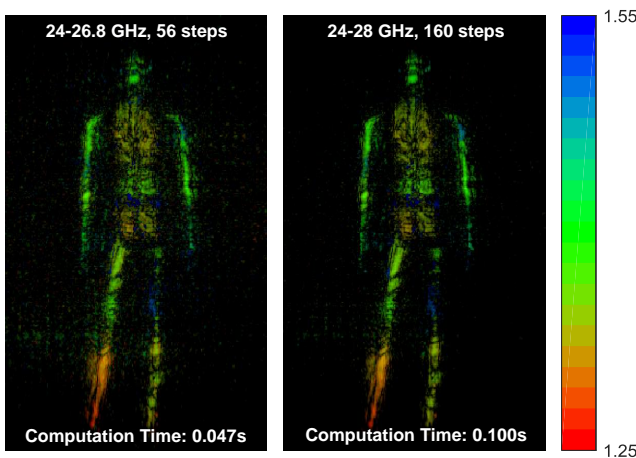

Fig. 12. Left: 24-26.8 GHz microwave image of metalized mannequin with no concealed items. Right: 24-28 GHz microwave image of the same scene.

from 24-29 GHz, and downconverts reflected signals to a 40 MHz IF. The IF is digitized by the DAQ, which samples at 160 MS/s, and provides on-board digital downconversion to baseband. In order to acquire a full body image and sample a scene as 1.5m (6x6 tile) array would, the antenna tile is mounted to an x-y scanner. To form the full aperture, it is moved to 36 positions, where it measures all transmit-receive returns.

To evaluate the single tile system, scenes with a metalized human phantom were imaged. Figs. 10 and 11 provides a photos and microwave images of the mannequin concealing a metal can in a backpack. In both images, the concealed can and features of the dummy are clearly visible. The images were taken from 24-28 GHz (160 steps) and formed with 21 depth slices. Additionally, the images are color-coded according to depth of maximum return. Fig. 12 depicts two microwave images of the dummy concealing no items. One image was formed with frequencies ranging from 24-26.8 GHz (56 steps) while the other was used data spanning 24-28 GHz (160 steps). As expected, image quality improves with increased bandwidth. Using a desktop computer with four Nvidia GeForce Titan X GPUs, the reconstruction time for these images was found to be 0.047s and 0.100s, respectively. This illustrates that video rate ($\geq 10Hz$) image reconstruction of a human-sized domain using cost-effective COTS computing hardware is feasible.

V. CONCLUSIONS

A multistatic array design and fast imaging technique for use in a video rate microwave imaging aperture were presented. Co-design of the array and fast imaging algorithm was discussed. Prototype hardware which forms a partition of an imaging aperture, was presented. Measurements with this prototype hardware showed that the array design can be used to form high-fidelity 3D microwave images. Further, it was shown that the fast imaging technique can reconstruct a human-sized image domain in $\leq 0.1s$ on cost-effective computing hardware, showing that video rate operation is feasible.

REFERENCES

[1] M. T. Ghasr, M. A. Abou-Khousa, S. Kharkovsky, R. Zoughi, and D. Pommerenke, "Portable real-time microwave camera at 24 ghz," *IEEE Transactions on Antennas and Propagation*, vol. 60, no. 2, pp. 1114–1125, 2012.

[2] E. C. Fear, X. Li, S. C. Hagness, and M. A. Stuchly, "Confocal microwave imaging for breast cancer detection: Localization of tumors in three dimensions," *IEEE Transactions on Biomedical Engineering*, vol. 49, no. 8, pp. 812–822, 2002.

[3] D. M. Sheen, D. L. McMakin, and T. E. Hall, "Three-dimensional millimeter-wave imaging for concealed weapon detection," *IEEE Transactions on Microwave Theory and Techniques*, vol. 49, no. 9, pp. 1581–1592, 2001.

[4] S. S. Ahmed, A. Schiessl, F. Gumbmann, M. Tiebout, S. Methfessel, and L. Schmidt, "Advanced microwave imaging," *IEEE Microwave Magazine*, vol. 13, no. 6, pp. 26–43, 2012.

[5] B. Gonzales-Valdes, C. Rappaport, and J. A. Martinez-Lorenzo, "On-the-move active millimeter wave interrogation system using a hallway of multiple transmitters and receivers," in *IEEE International Symposium on Antennas and Propagation*, 2014, pp. 1107–1108.

[6] M. Karaman, I. O. W. anf O. Oralkan, and B. T. Khuri-Yakub, "Minimally redundant 2-d array designs for 3-d medical ultrasound imaging," *IEEE Transactions on Medical Imaging*, vol. 28, no. 7, pp. 1051–1061, 2009.

[7] R. J. Kozick and S. A. Kassam, "Synthetic aperture pulse-echo imaging with rectangular boundary arrays," *IEEE Transactions on Image Processing*, vol. 2, no. 1, pp. 68–79, 1993.

[8] Y. Alvarez, Y. Rodriguez-Vaqueiro, B. Gonzalez-Valdes, S. Mantzavinos, C. M. Rappaport, F. Las-Heras, and J. A. Martinez-Lorenzo, "Fourier-based imaging for multistatic radar systems," *IEEE Transactions on Microwave Theory and Techniques*, vol. 62, no. 8, pp. 1798–1810, 2014.

[9] X. Zhuge and A. G. Yarovoy, "A sparse aperture mimo-sar-based uwb imaging system for concealed weapon detection," *IEEE Transactions on Geoscience and Remote Sensing*, vol. 49, no. 1, pp. 509–518, 2011.

[10] G. L. Charvat, L. C. Kempel, E. J. Rothwell, C. M. Coleman, and E. L. Mokole, "A through-dielectric ultrawideband (uwb) switched-antenna-array radar imaging system," *IEEE Transactions on Antennas and Propagation*, vol. 60, no. 11, pp. 5495–5500, 2012.

[11] I. D. Longstaff, H. Ashoka, and T. Kilpatrick, "Mimo radar developments at teledyne australia," in *International Conference on Radar*, 2013, pp. 184–187.

[12] M. Arakawa, *Computational Workloads for Commonly Used Signal Processing Kernels*, ser. Project report, MIT Lincoln Laboratory, 2006. Lincoln Laboratory, Massachusetts Institute of Technology, 2003.

[13] W. F. Moulder, J. J. Majewski, C. M. Coldwell, J. D. Krieger, and J. S. Herd, "Switched antenna array tile for real-time microwave imaging aperture," in *IEEE International Symposium on Antennas and Propagation*, 2016.